Available online at BCREC website: https://bcrec.id

Bulletin of Chemical Reaction Engineering & Catalysis, 18 (4) 2023, 659-674

Research Article

# Treatment of Methylene Blue Using Ni-Al/Magnetite Biochar Layered Double Hydroxides Composite by Adsorption

**Zaqiya Artha Zahara[1], Idha Royani[2], Neza Rahayu Palapa[2], Risfidian Mohadi[3,4], Aldes Lesbani[3,4,*]**

[1]*Magister Program in Environment Management, Sriwijaya University, Jl. Padang Selasa No. 524 Ilir Barat 1, Palembang, South Sumatra, Indonesia*
[2]*Graduate School, Faculty of Mathematics and Natural Science, Sriwijaya University, Jl. Palembang-Prabumulih, Km. 90-32, Ogan Ilir, South Sumatera, Indonesia*
[3]*Research Center of Inorganic Materials and Complexes, Universitas Sriwijaya, Palembang, 30139, Indonesia*
[4]*Master Program of Material Science, Graduate School Universitas Sriwijaya, Palembang, 30139, Indonesia*

*Received: 1st October 2023; Revised: 15th November 2023; Accepted: 16th November 2023*
*Available online: 17th November 2023; Published regularly: December 2023*

## Abstract

Methylene blue dye is hard to degrade and requires treatment using Ni-Al Layered double hydroxides (LDHs) modified with magnetite biochar (MBC) to form Ni-Al/magnetite biochar composite in overcoming environmental pollution. Material attainment was identified by characterization using X-Ray Diffraction (XRD), Fourier Transform – Infra Red (FT-IR), Branuer Emmet Teller (BET), Scanning Electron Microscopy – Energy Dispersive X-Ray (SEM-EDX) and Vibration Sample Magnetometer (VSM). XRD characterization displays angle 2θ at 11°, 60° is a typical angle of LDH, and angles 22° and 35° of magnetite biochar. FT-IR characterization analysis at wavelength 1381 $cm^{-1}$ for $NO_3^-$ group and M-O group at wave number 700 $cm^{-1}$. C-H group on biochar at 1404 $cm^{-1}$ and wave number 586 $cm^{-1}$ for Fe-O group. BET characterization analysis of Ni-Al/MBC has a large surface area and pore volume of 127.310 $m^2/g$ and 0.1950 $cm^3/g$. SEM characterization analysis of Ni-Al/MBC has large, coarse pores and non-uniform shape, EDX data shows that there are forming elements such as Ni, Al from LDH and, Fe, C elements from magnetite biochar. pH, kinetics, isotherms, and thermodynamics become influential in adsorption processes. The adsorption capacity of the composite reaches 68.493 mg/g by following the Langmuir equation and adsorption kinetics refers to the Pseudo Second Order (PSO) equation. Adsorption continuity is spontaneous and endothermic. Ni-Al/MBC has stability in the process of adsorbent regeneration up to five adsorption cycles and, therefore can be used as a potential adsorbent in the treatment of methylene blue dye in aqueous environmental pollution.



***Keywords***: Ni-Al LDHs; Magnetite Biochar; Composite; Methylene Blue; Regeneration

***How to Cite***: Zahara, Z. A., Royani, I., Palapa, N. R., Mohadi, R., Lesbani, A. (2023). Treatment of Methylene Blue Using Ni-Al/Magnetite Biochar Layered Double Hydroxides Composite by Adsorption. *Bulletin of Chemical Reaction Engineering & Catalysis*, 18(4), 659-674 (doi: 10.9767/bcrec.20049)

***Permalink/DOI***: https://doi.org/10.9767/bcrec.20049

## 1. Introduction

The consumption of dyes has grown rapidly along with the development of various products, especially textiles. The environmental impact of industrial development is untreated waste, resulting in water pollution. Retrieved from [1] dyeing and finishing products from the textile industry generate 20,000 tonnes of dyestuffs to discharge into water bodies. Non-biodegradable textile dyes such as cationic dye methylene blue are contributing to excess Biochemical Oxygen

* Corresponding Author.
Email: aldeslesbani@pps.unsri.ac.id (A. Lesbani)

Demand (BOD) and Chemical Oxygen Demand (COD) concentrations in water bodies [2]. Methylene blue has an aromatic heterocyclic structure ($C_{16}H_{18}ClN_3S$) with a molecular weight of 319.85 g/mol [3]. The blue color of methylene blue comes from the interaction of the chromophore group conjugated to the N-S group located within the central aromatic heterocyclic [4]. Conversely, the auxochrome group is an N-containing component with an unbound electron pair located in the benzene ring [5]. Disposal of untreated methylene blue can have adverse health effects on humans, such as kidney, tissue necrosis, cyanosis, difficulty in breathing, yellow jaundice, and vomiting [6,7].

Numerous chemical, physical, and biological methods have been employed in dye treatment, including ion exchange [8], membrane filtration [9], coagulation-flocculation [10,11], chemical oxidation [12], photo-degradation [13], and sludge ponds [14]. However, they are not cost-effective and provide waste products after processing [15]. The adsorption method was chosen considering its advantages, such as easy and cheap equipment, efficiency and effectiveness in dye treatment, fast reaction kinetics, and re-generating adsorbent [16]. Adsorbents that have been developed in adsorption methods include silica gel [17], zeolite [18], clay [19], fly ash [20], activated carbon [21], magnetic [22], and layered double hydroxy [23].

Layered double hydroxide (LDH) becomes a prestigious adsorbent because it has a unique structure in which anion interlayer can be exchanged with other ions such as polyoxometalate, and has a large surface area [24]. LDH has a general formula $[M_{1-x}^{2+}M_x^{3+}(OH)_2]^{x+}[A_{x/n}]^{n-}mH_2O$, where $M^{2+}$ and $M^{3+}$ are divalent and trivalent metal ions, respectively, and $A_n^-$ is the interlayer anion [25]. The commonly used ratio in LDH formation is 2-3:1, this allows the formation of trivalent metal hydroxide ($M(OH)_3$) [26], and preparation methods such as co-precipitation, hydrothermal, sol-gel, and electrodeposition [27]. Repeated use of LDH can cause the coating to undergo exfoliation, reducing the adsorption capacity and thus requiring modification with materials in the form of composites [28]. Tang *et al*. [29] research found that magnetite could be used as one of the composite materials. Zn-Al/magnetite can adsorb malachite green dye with a maximum capacity of 850.93 mg/g and can be regenerated up to 4 cycles. Cu-Al adsorbent modified with biochar by Wijaya *et al*. [30] can adsorb procion red up to 93.458 mg/g at high temperatures with the Langmuir isotherm model, and the composite has a stable structure for up to 5 adsorption cycles.

In the study reviewed by Pelalak *et al*. [31], it was found that when Fe-Al LDH is enhanced with biochar, it can effectively eliminate phenol organic pollutants, achieving an impressive 85.28% removal rate. This efficient removal process occurs within an optimal timeframe of 120 minutes. The mechanism behind this degradation involves the utilization of $H_2O_2$, which accepts electrons from Fe(II), initiating a redox reaction that results in the generation of Fe(III) on the LDH surface. This Fe(III) presence on the LDH surface facilitates the oxidation of phenol groups, particularly the hydroxide ions ($OH^-$). The findings from Karim *et al*. [32] study, as mentioned in Shou *et al*. [33] research, suggest that MgAl-$Fe_3O_4$ holds promise as a water pollution adsorbent for Co(II) at a concentration of 0.5 g/L. Moreover, the incorporation of LDH with semiconductors like $Fe_3O_4$ can enhance photocatalytic efficiency by effectively segregating light-induced electrons ($e^-$) and holes ($h^+$). Modification LDH with magnetite to improve possesses high chemical stability that allows it to be used repeatedly in the treatment of dye wastewaters with less cost, and low toxicity to the environment [34]. Biochar has the advantage of being modified with LDH is renewable and widely found everywhere, and has a large pore surface so that it can increase the surface area [35].

This paper researches the modification of LDH $M^{2+}$ metal cation of Ni and $M^{3+}$ metal cation of Al with magnetite ($Fe_3O_4^-$) biochar material which is applied for methylene blue dye treatment in an aqueous solution. Synthesis of LDH using coprecipitation method while preparation of composite combining by hydrothermal method. X-Ray Diffraction (XRD), Fourier Transform – Infra Red (FT-IR), Branuer Emmet Teller (BET), Scanning Electron Microscopy – Energy Dispersive X-Ray (SEM-EDX) and Vibration Sample Magnetometer (VSM) characterized adsorbents and also examined the materials regarding structural stability for repeated adsorbent applications in terms of the regeneration process. The adsorption process is affected by pH pzc, kinetics, isotherms, and thermodynamics.

## 2. Materials and Methods

### 2.1 Chemicals

The chemicals used included distilled water, aluminum nitrate nonahydrate $Al(NO_3)_3.9H_2O$ (Sigma-Aldrich, 375.13 g/mol), hydrochloric acid HCl 37% (MallinckrodtAR®, 37%), iron (III)

chloride $FeCl_3$ (Merck kGaA 162.20 g/mol), iron(II) sulfate $FeSO_4$ (Smart-Lab 278.01 g/mol), biochar, methylene blue ($C_{16}H_{18}ClN_3S$), sodium hydroxide NaOH (EMSURE® ACS, 40 g/mol), sodium carbonate $Na_2CO_3$ (EMSURE® ACS, 105.99 g/mol), nickel nitrate hexahydrate $Ni(NO_3)_2.6H_2O$ (EMSURE® ACS, 290.81 g/mol).

## 2.2 Methods

### 2.2.1 Synthesis of Ni-Al LDH

Ni-Al LDH was produced through the co-precipitation method. Initially, 50 mL of a 2 M NaOH solution was combined with 100 mL of a 0.3 M $Na_2CO_3$ solution. Subsequently, 100 mL of a 0.25 M $Al(NO_3)_3.9H_2O$ solution and 100 mL of a 0.75 M $Ni(NO_3)_2.6H_2O$ solution were added drop by drop to achieve a pH level of 10, 2 M NaOH solution was used for pH adjustment. The resulting mixture was stirred for 17 hours at a temperature of 80 °C. Afterward, the residue obtained underwent filtration, followed by washing with distilled water, and finally, it was dried in an oven at 100 °C for 24 hours.

### 2.2.2 Synthesis of magnetite biochar

A quantity of 1 gram of $FeCl_3$ was dissolved in 3 mL of distilled water, and simultaneously, 0.6 gram of $FeSO_4.7H_2O$ was dissolved in 3 mL of distilled water. The resulting solutions were combined and then introduced to 1 gram of biochar, and the mixture was gently stirred at room temperature for 3 hours. Subsequently, 3.5 mL of $NH_3$ solution was slowly added drop by drop to the mixture, and it was stirred at 75 °C for 30 minutes. The resulting solution was transferred into a 100 mL hydrothermal stainless steel autoclave. The mixture was heated to 150 °C and maintained at this temperature for 3 hours. The solid product of magnetite biochar was separated through filtration and subsequently dried at 100 °C.

### 2.2.3 Preparation of Ni-Al/magnetite biochar

A mixture was prepared by combining 30 mL of a 2 M $Na_2CO_3$ solution with 15 mL of 2 M NaOH and stirring it. Subsequently, 30 mL of 0.25 M $Ni(NO_3)_2.6H_2O$ (containing $M^{2+}$ ions) and 30 mL of 0.75 M $Al(NO_3)_3.9H_2O$ solution were added, to achieve a pH level of 10, 2 M NaOH was slowly added. The resulting mixture was stirred for 17 hours at a temperature of 70 °C. After that, 3 gram of biochar were introduced into the mixture and stirred for 30 minutes at 70 °C, resulting in the formation of a Ni-Al/biochar LDH solution. In a separate process, 2 gram of $FeCl_3$ were dissolved in 3 mL of distilled water, and simultaneously, 1.6 gram of $FeSO_4.7H_2O$ were dissolved in 3 mL of distilled water. This solution was stirred for 3 hours at room temperature. The resulting mixture was slowly dripped with 7 mL of $NH_3$ solution and stirred at 75 °C for 30 minutes to create a magnetite solution. Added magnetite solution to the Ni-Al LDH solution and stirred for 30 minutes. The resulting solution was transferred into a 100 mL hydrothermal stainless steel autoclave and heated at 150 °C for 3 hours. The solid product obtained was filtered, washed with distilled water, and dried in an oven at 100 °C for 24 hours.

### 2.2.4 Characterizatios

Ni-Al LDH, magnetite biochar, and Ni-Al/magnetite biochar composite were characterized by XRD for angle 2θ with Rigaku Miniflex-6000. Groups on the materials were using a Shimadzu Prestige-21 FT-IR spectrophotometer. Surface area using BET characterization with $N_2$ adsorption-desorption equipment Quantachrome instruments. Morphology and elements using SEM-EDX SU 8000 series. Measurement of the magnetic value of the material using VSM type OXFORD VSM 1.2H 250 - P2F. Absorbance value measurements using a Biobase BK-UV 1800 PC UV-Vis spectrophotometer with a maximum absorbance wavelength of 665 nm.

### 2.2.5 Desorption and regeneration materials

The desorption and regeneration process is done by adding 15 mL of methylene blue to 0.15 gram of adsorbent material and stirring for 2 hours. The filtrate obtained after stirring is measured using a UV-Vis spectrophotometer, and the adsorbent is dried for desorption. The desorption process was carried out by adding 15 mL of equates to the dried adsorbent and putting it into the ultrasonic device for 20 minutes. The obtained filtrate measured its absorbance value, and the adsorbent was dried again for subsequent regeneration. The desorption and regeneration process is repeated for five cycles.

### 2.2.6 Adsorption treatment of methylene blue

pH pzc determination was carried out by adding 15 mg of adsorbent into 15 mL of 0.1 M NaCl, which had previously been adjusted with variations of pH of 2, 3, 4, 5, 6, 7, 8, 9, 10, and 11. The solution was then stirred with a magnetic stir bar for 24 hours, then the pH was

measured again after stirring, and a graph was made of the relationship between initial pH and pH after stirring with a pH meter. Kinetic, isotherm, and thermodynamic adsorption processes using 15 mL of methylene blue concentration of 30 ppm were added to 0.015 gram of adsorbent material, the kinetic adsorption processes stirring using time variations of 0, 5, 10, 20, 30, 50, 70, 90, 120, and 180 minutes, the absorption values obtained on the slope of the function graph and the corresponding value of the adsorption. The isotherm and thermodynamic adsorption processes use concentration variations of 5, 15, 30, 45, and 60 mg/L with temperature variations of 30, 40, 50, and 60 °C, stirring processes using a stirrer at the optimum time; the filtrate is measured using a UV-vis spectrophotometer at 665 nm wavelength. Furthermore, record the absorbance values for calculation in MS Excel and create a graphical representation depicting the relationship between concentration and temperature.

## 3. Results and Discussion

### 3.1 Regeneration Process

The regeneration process is intended to determine the adsorbent's ability in repeated use, therefore saving costs and being friendly to the environment. Ultrasonic devices are used in the desorption process due to the working principle of high-frequency wave propagation in liquid media. Liquid is propagated as a sound medium with high-frequency ultrasonic waves that produce microscopic vibrations so that impurities that are firmly attached can be released more easily [36]. The vibration affecting liquid in the container has a strong shock force, resulting in all impurities attached to the adsorbent material being removed. Regeneration and desorption procedures were applied five times, resulting in the percent adsorbed graph shown in Figure 1. Percentage adsorption ability for five cycles decreased drastically as regeneration cycles increased for the following adsorbents: Ni-Al from 72.111; 68.674; 39.683; 28.660; and 14.395 %; magnetite biochar from 87.573; 79.762; 66.145; 56.808; and 31.384%; Ni-Al/magnetite biochar tends to be stable in decreasing the adsorption percent start from 96.587; 95.330; 93.293; 80.311; 58.494 %. The lower % adsorption is due to the solvent's inability to completely remove dye molecules bound to materials into the solution, resulting in a diminishing number of adsorption sites on the material as the number of cycles increases.

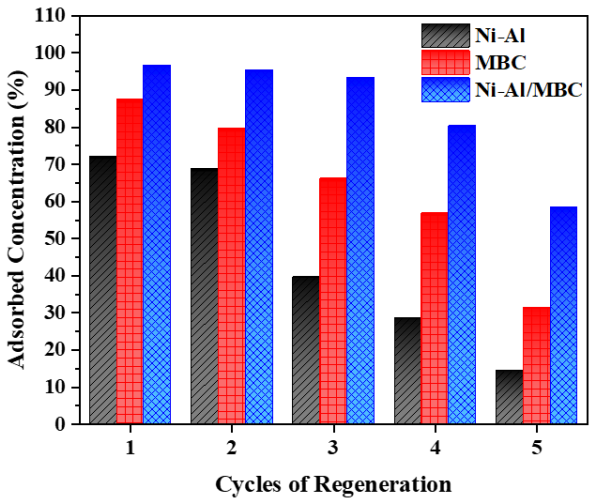


Figure 1. Regeneration cycle of adsorbents Ni-Al LDH, magnetite biochar, Ni-Al/magnetite biochar against methylene blue

### 3.2 XRD Characterization Analysis

XRD analysis can serve as a valuable analytical tool for understanding changes in the structure and crystal properties of adsorbent materials during the regeneration process. This can aid in improving the efficiency of the regeneration process, as well as in gaining insight into the regeneration mechanisms, as observed through significant alterations in the crystal structure or material phases displayed at the 2θ angle. XRD analysis of Ni-Al LDH, magnetite biochar, and Ni-Al/magnetite biochar is shown in Figure 2. Diffraction peaks of Ni-Al at 2θ angles were observed at 11.57° (003), 22.91° (006), 35.04° (012), 39.73° (015), and 61.9° (110). These diffraction peaks align with the expected characteristic angles of the layered

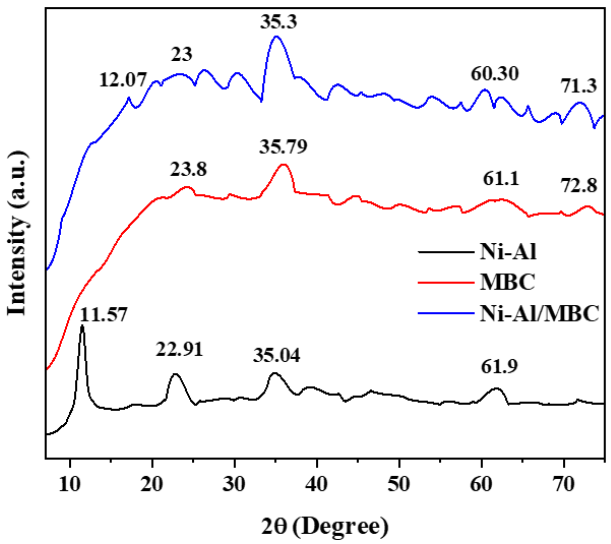


Figure 2. Characterization of adsorbents Ni-Al LDH (a) Magnetite biochar (b) and Ni-Al/magnetite biochar (c) using X-Ray Diffraction

double hydroxide: angles between 9° to 11° indicate a layered structure, 35° corresponds to metal oxides, and 60° signifies the presence of anion interlayers. This finding is consistent with the research conducted by *Hu et al.* [37], which reported diffraction angles for the Ni-Al LDH at 11.7° (003), 23.5° (006), 35.1° (012), 39.7° (015), 47.3° (018), 61.2° (110), and 62.5° (113), by the JCPDS No. 15-0087 data. pada 23,8°(002); 35,79°(311); 61,1°(110); dan 72,8°(533). The diffractogram of the magnetite biochar material showed an amorphous crystallinity; 2θ angles of the magnetite biochar material were observed at 23.8° (002), 35.79° (311), 61.1° (440), and 72.8° (533). The expected 2θ angle for magnetite biochar typically appears around 22°, indicating the presence of carbonaceous material, while magnetite is indicated at 2θ angles of 30-35° and 62-63°. The diffractogram of magnetite biochar obtained by Din *et al.* [38] displayed 2θ angles at 30°, 35.5°, 44°, 56.3°, and 62.5°, each corresponding to indices in sequence (220), (311), (400), (422), and (440), confirming that the magnetite biochar material aligns with JCPDS No.19-0619 data. The results of the analysis of the composite material of Ni-Al/magnetite biochar represent a combination of diffraction angles from the Ni-Al LDH and magnetite biochar, 2θ angles observed were 12.07° (003), 23° (006), 35.3° (311), 60.30° (440) and 71.3° (533). Diffractogram of Ni-Al, magnetite biochar, and Ni-Al/magnetite biochar presented indicates successful synthesis and preparation of these materials.

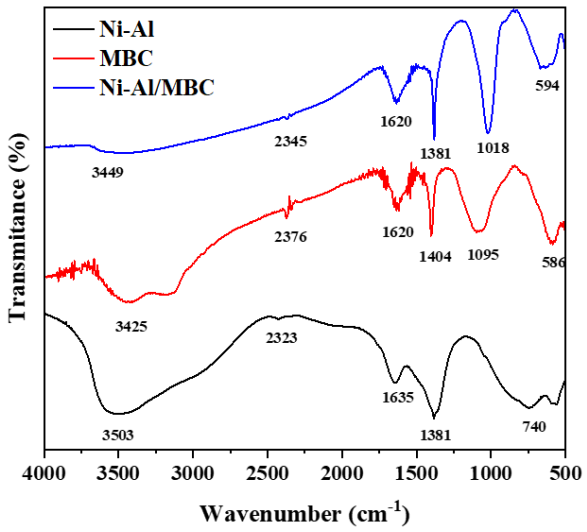


Figure 3. Characterization of adsorbents Ni-Al LDH (a) Magnetite biochar (b) and Ni-Al/magnetite biochar (c) using Fourier Transform – Infra Red

### 3.3 FT-IR Characterization Analysis

FT-IR analysis to determine chemical bonds, such as functional groups on a sample from liquid to solid to gas, using an FT-IR spectrophotometer. Results of FT-IR analysis include wave numbers and the presence of vibrational peaks. Accordingly, a connection between FTIR and regeneration processes is that FTIR can determine changes in functional groups on the adsorbent during regeneration, both before and after, aiding in optimizing the process and ensuring efficiency in recovering adsorbent capacity. FT-IR spectra of Ni-Al, magnetite biochar, and Ni-Al/magnetite biochar materials are shown in Figure 3. Ni-Al LDH has a peak vibration at wave number 3503 $cm^{-1}$ indicating the stretching of the O-H group on water molecules with strong intensity and broad vibrations. The wave number 1635 $cm^{-1}$ indicates the bending vibration of O-H with sharp intensity. A typical FT-IR spectrum of LDH is present at wave number 1381 $cm^{-1}$, which indicates the presence of the $NO_3^-$ group with solid and sharp intensity. M-O (Ni-O and Al-O) is present at wave 740-347 $cm^{-1}$. The results of Siregar *et al.* [39] reveal that the LDH vibrational peaks at wave numbers 3464 $cm^{-1}$, 1635 $cm^{-1}$, 1381 $cm^{-1}$ , and 748 $cm^{-1}$.

FT-IR spectrum of magnetite biochar displays a widened wave number of 3425 $cm^{-1}$, signifying the presence of O-H groups from water molecules. The C≡C stretch is present at 2376 $cm^{-1}$ and the C=O carbonyl group is at 1620 $cm^{-1}$. Biochar has a C-H carbon group at wave number 1404 $cm^{-1}$ with strong and sharp intensity and C-O vibration at 1095 $cm^{-1}$. Wave number indicating the presence of Fe-O magnetite is found at wave number 586 $cm^{-1}$. The FTIR spectrum of Din *et al.* [40] showed a broad band at 3499 $cm^{-1}$, 1725 $cm^{-1}$, and 1433 $cm^{-1}$ in magnetite biochar in aliphatic groups (C-H), 1364 $cm^{-1}$ is caused by strain (C-O). Peaks of vibration at 779 $cm^{-1}$, 1085 $cm^{-1}$, and 529-552 $cm^{-1}$ can be attributed to stretching vibration (Fe-O) suggesting that it is a magnetic material. Ni-Al/magnetite biochar composite exhibits a combined spectrum of the FT-IR spectra of Ni-Al and magnetite biochar. The occurrence of the O-H group from water molecules shifted wave number to 3449 $cm^{-1}$. Hence, the presence of $Fe_3O_4$ groups in the composite can weaken hydrogen bonds in the structure [41].

### 3.4 VSM Characterization Analysis

VSM can be utilized to comprehend the magnetic properties of materials and their cor-

relation with the regeneration process by monitoring changes in the physical and chemical characteristics that impact the magnetic properties of the adsorbent material after regeneration. Furthermore, VSM can be employed for investigating the modification of LDH with magnetite in understanding the kinetics, isotherms, and thermodynamics that influence the adsorption capacity. Figure 4 depicts magnetization curve M with magnetic field strength H. The Magnetic field generated by magnetite biochar is 20.201 kOe with a magnetization saturation value of 13.04 emu/g. The obtained results are similar to the results of [42]. VSM analysis results from the Ni-Al/magnetite biochar LDH composite with a magnetic field value of 20.216 kOe, followed by a magnetization saturation result of 8.35 emu/g. The saturation value of magnetite biochar magnetization is greater than composite influenced by $Fe_3O_4$ content, grain size, and density, so an increase in magnetization value can lead to an increase in crystallinity structure [43]. Magnetite biochar and Ni-Al/magnetite biochar composite have superparamagnetic properties S-shaped and pass through the zero point, bringing wide applications in treating the environment, especially removing chemical contaminants, and dyes.

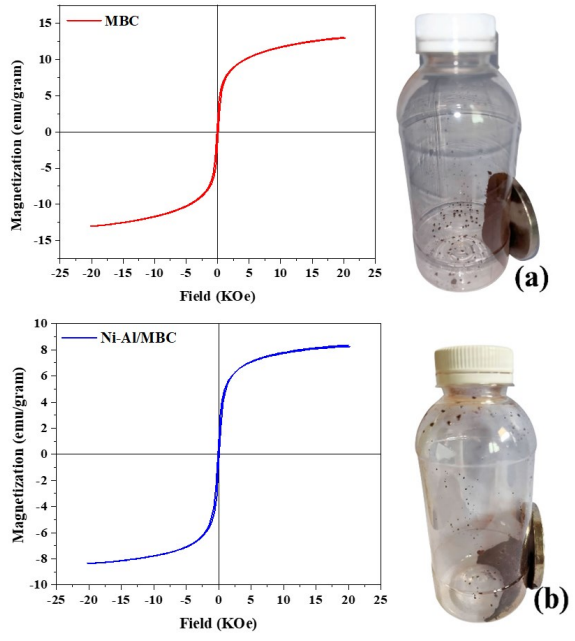


Figure 4. VSM magnetization curve and (a) Magnetite Biochar (b) Ni-Al/magnetite biochar separation performance

3.5 Adsorption Experiment

3.5.1 Effect of pH pzc

The pH pzc method was used to assess the materials state of Ni-Al, magnetite biochar, and Ni-Al/magnetite biochar as zero charged or uncharged. Figure 5 presents a graph of pH pzc from Ni-Al LDH, magnetite biochar, and Ni-Al/magnetite biochar LDH composite. It is seen from the intersection of the line between the final pH of the material and the initial pH. The line intersection that occurs at pH pzc of Ni-Al LDH is at pH 7.6, magnetite biochar is at pH 6.4, while Ni-Al/magnetite biochar LDH composite results in pH pzc at pH 8. Therefore, pH > pH pzc indicates that the adsorbent surface is negatively charged, so anionic dye adsorption is difficult to absorb. However, at pH < pH pzc, the adsorbent surface becomes positively charged, thus increasing the adsorption capacity due to the attractive force between the positive charge of the adsorbent and the negative charge of the dye [44].

3.5.2 Effect of kinetic studies

Time variation serves a purpose in determining the optimum time to perform adsorption process and analyzing the reaction kinetics as time progresses. The optimum time graph for adsorbents Ni-Al, magnetite biochar, Ni-Al/magnetite biochar are shown in Figure 6. The increase and stability of the adsorption capacity of methylene blue dye with Ni-Al LDH occurred at 90 min. The optimum time obtained by magnetite biochar and Ni-Al/magnetite biochar LDH composite was 70 min and 50 min, respectively. The determination of adsorption kinetics aims to uncover the

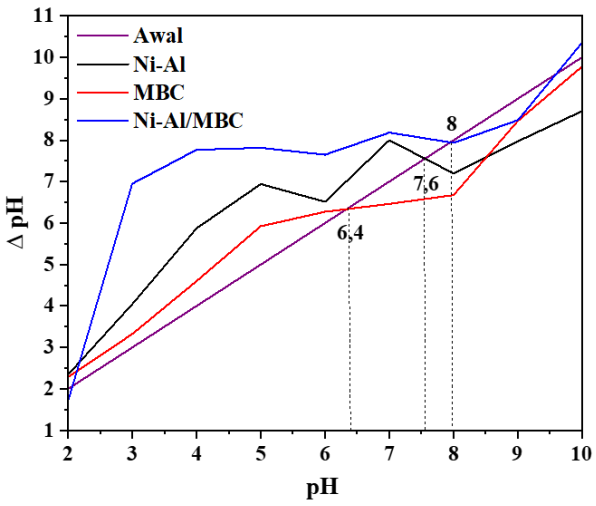


Figure 5. Effect of pH pzc

adsorption mechanism by analyzing and understanding processes of interaction that occur between adsorbent and adsorbate, as well as evaluating how the adsorbate transfers from the solution to the surface or within the structure of adsorbent at the molecular level.

The determination of pseudo-first-order and pseudo-second-order kinetics is based on the slope and intercept of the linear plot, while exhibiting regression values approaching 1. Subsequently, the smallest values of $k_1$ and $k_2$, also calculated $Q_e$ value closely approximates the experimental $q_e$ value, are considered [44]. Data presented in Table 1 indicates that all three adsorbents, namely Ni-Al, magnetite biochar, and Ni-Al/magnetite biochar, follow the pseudo-second-order kinetic equation with R-squared ($R^2$) values of 0.9937, 0.888, and 0.9993, respectively. Furthermore, the calculated $k_2$ values are smaller than $k_1$, namely 0.0020, 0.0006, and 0.0097, respectively. It is also evident that experimental $q_e$ values closely resemble calculated $q_e$ values in the Pseudo Second Order (PSO) model compared to the Pseudo First Order (PFO) model.

### 3.5.3 Effect of isotherm and thermodynamic studies

The study of isotherms and thermodynamics in the context of adsorption has several main objectives, which are to identify the types of interactions occurring during the adsorption process, determine the maximum adsorption capacity of the adsorbent for the dye, ascertain whether the adsorption mechanism is physical or chemical in nature, and to determine thermodynamic constants such as enthalpy, degree of disorder, and Gibbs free energy. Figure 7,

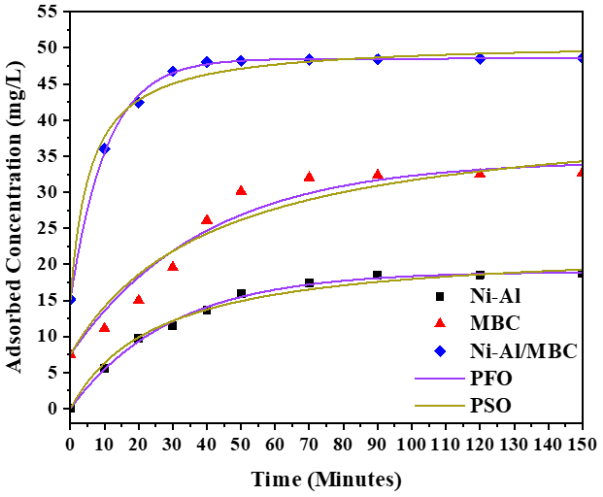


Figure 6. Curves of Pseudo First Order (PFO) and Pseudo Second Order (PSO)

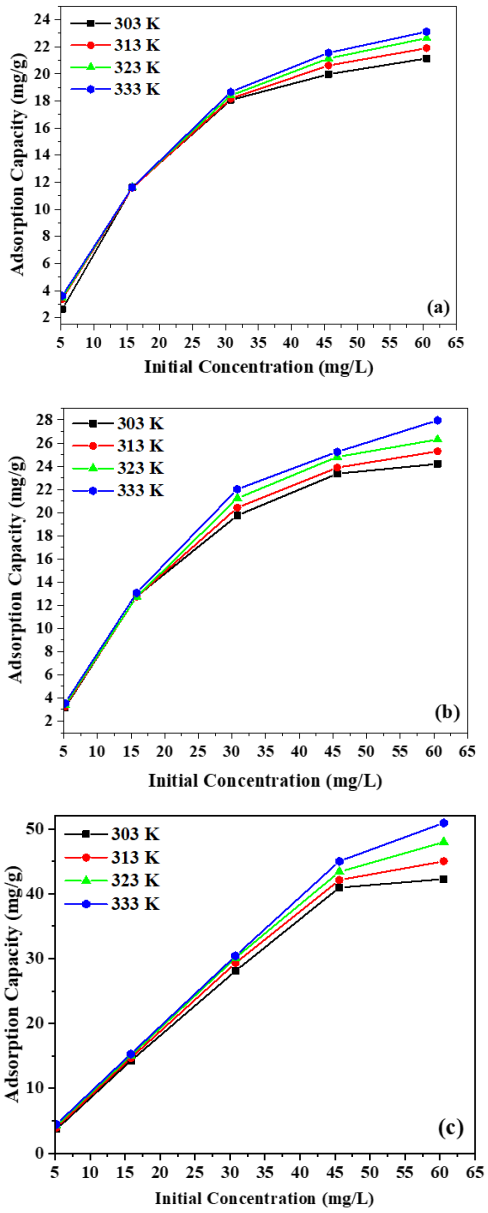


Figure 7. Effect of concentration and temperature curves for adsorption methylene blue using (a) Ni-Al LDH (b) Magnetite Biochar and (c) Ni-Al/magnetite biochar

Table 1. Adsorption kinetic of methylene blue

| Kinetic model | Parameter | Adsorbents | | |
|---|---|---|---|---|
| | | Ni-Al LDH | MBC | Ni-Al/MBC |
| Pseudo - first order | $Q_{e,exp}$ (mg/g) | 18.839 | 21.555 | 29.401 |
| | $Q_{e,calc}$ (mg/g) | 31.776 | 54.150 | 11.516 |
| | $k_1$ ($min^{-1}$) | 0.0493 | 0.0569 | 0.0491 |
| | $R^2$ | 0.874 | 0.751 | 0.8466 |
| Pseudo - second order | $Q_{e,exp}$ (mg/g) | 18.839 | 21.555 | 29.401 |
| | $Q_{e,calc}$ (mg/g) | 21.834 | 30.303 | 30.120 |
| | $k_2$ ($min^{-1}$) | 0.0020 | 0.0006 | 0,0097 |
| | $R^2$ | 0.9937 | 0.888 | 0.9993 |

adsorption of methylene blue with Ni-Al 7 (a), magnetite biochar 7 (b), and Ni-Al/magnetite biochar 7 (c) adsorbents, show that the concentration of dye solution increases and is directly proportional to adsorption capacity. The reason for this is that at high temperatures, adsorbent and adsorbate molecules collide and become reactive, making it easier for interactions to occur in the treatment of methylene blue. Equilibrium is reached when the adsorbent's ability to adsorb dye has reached a saturation phase, as evidenced by a plateau in the graph or a lack of significant further increase.

Table 2 represents data from temperature and concentration calculations in determining Langmuir and Freundlich equations. The results show that Ni-Al, magnetite biochar, and Ni-Al/magnetite biochar in the adsorption of methylene blue dye follow Langmuir equation. The values of $R^2$ are closer to 1 compared to $R^2$ of the Freundlich equation. $Q_{max}$ of Ni-Al/magnetite biochar composite has a greater capacity of 68.493 mg/g than the forming precursors, namely Ni-Al LDH of 33.003 mg/g and magnetite biochar of 37.736 mg/g, and also supported by the value of the Langmuir equilibrium constant less than one which means that monolayer adsorption is more optimal. The establishment of Langmuir and Freundlich equations is seen from linear plots with $R^2$ values close to 1 or > 0.9. Adsorption with the Langmuir equation is monolayer adsorption (only one adsorbate molecule can be adsorbed on each adsorbent site), which means a large surface area will result in a high adsorption capacity, and the adsorbent sites are homogeneous. Adsorption modeled by the Freundlich equation occurs in multilayers on heterogeneous sites [45]. $Q_{max}$ enhances with increasing temperature because the mobility of dye molecules increases resulting in an elevated diffusion rate into the adsorption site [46]. Temkin isotherm model describes the adsorption of molecules on the surface of solids with changes in molecular concentration over time marked by a linear decrease in the curve. The results calculated for the Temkin isotherm show that the $K_T$ value with increasing temperature is getting bigger. This means that the stronger adsorption on the adsorbent layer [47]. The Dubinin-Radushkevich (D-R) isotherm links the adsorption mechanism to the free energy of adsorption [48]. The free energy results shown in Table 2 that the methylene blue adsorption process with the three materials is assumed to occur by chemisorption with the largest energy value in the Ni-Al/MBC composite 1674.616 kJ/mol. The lack of the D-R model is the inability to fit low-concentration adsorbates thus the $Q_m$ value is smaller than $q_e$ of methylene blue dye. Table 3 presents different maximum adsorption capacities of several adsorbents in terms of the adsorption of methylene blue dye.

Thermodynamic results of methylene blue dye with the three adsorbents are presented in Table 4. Thermodynamic data indicate that as the concentration increases, the enthalpy value decreases. Adsorption processes for Ni-Al LDH, magnetite biochar, and Ni-Al/magnetite biochar LDH composites are endothermic and occur spontaneously. Based on the literature by Sahmoune *et al*. [49], a decrease in the ΔG° value with increasing temperature indicates the spontaneity of the process at higher temperatures. Endothermic behavior is also evident from the positive value of the enthalpy change (+ΔH°), and it is directly proportional to the change in entropy (ΔS°). Physisorption processes are reversible and involve weak Van der Waals attractions between adsorbate (dye) and adsorbent surface. On the other hand, chemisorption occurs due to chemical bonding between the adsorbent and adsorbate, and it is irreversible.

Enthalpy values lower than 40 kJ/mol for Ni-Al, magnetite biochar, and Ni-Al/magnetite biochar, respectively, at 15.575, 16.262, and 24.213 kJ/mol indicate the presence of weak Van der Waals interactions, hydrogen bonding, electrostatic forces, and ion exchange [60]. The fluctuation in enthalpy value may result from external factors affecting the system during the adsorption process. From the table, at a high concentration of 60 mg/L for Ni-Al and

Table 3. Maximum adsorption capacity of methylene blue and comparison with other research

| Adsorbent | $Q_{max}$ (mg/g) | Reference |
|---|---|---|
| $Mn_3O_4$-$Bi_2O_3$ | 3.12 | [50] |
| Carbonized peanut shell | 5.34 | [51] |
| Maghemite | 26.5 | [52] |
| Zeolite | 21.189 | [53] |
| Coconut shell | 2.97 | [54] |
| Chitosan | 15.337 | [55] |
| Hydroxyapatite | 11.21 | [56] |
| Kraft softwood lignins from LignoBoost | 30.67 | [57] |
| Cellulose Microcrystalline | 27.78 | [58] |
| Magnetite Humic Acid | 156.250 | [59] |
| NiAl LDH | 33.003 | This work |
| Magnetite Biochar | 37.736 | This work |
| Ni-Al/magnetite biochar | 68.493 | This work |

Table 2. Adsorption isotherm of methylene blue

| Adsorbents | Tempera-ture (K) | Adsorption Isotherm Model | | | | | | | | | | | | |
|---|---|---|---|---|---|---|---|---|---|---|---|---|---|---|
| | | Freundlich | | | Langmuir | | | Temkin | | | Dubinin -Radukevisch (D-R) | | | |
| | | n | $K_F$ | $R^2$ | $Q_m$ | $K_L$ | $R^2$ | $B_T$ | $K_T$ | $R^2$ | $Q_m$ | $K_D$ | $R^2$ | $E$ |
| Ni-Al LDH | 303 | 1.562 | 2.598 | 0.723 | 30.675 | 0.067 | 0.7837 | 6.245 | 0.983 | 0.855 | $2.94x10^{-6}$ | 21.619 | 0.9715 | 412.519 |
| | 313 | 1.590 | 2.960 | 0.842 | 31.348 | 0.081 | 0.8754 | 6.641 | 1.031 | 0.913 | $2.09x10^{-6}$ | 21.972 | 0.9959 | 488.876 |
| | 323 | 1.603 | 3.225 | 0.7945 | 32.680 | 0.086 | 0.8909 | 6.922 | 1.086 | 0.926 | $1.74x10^{-6}$ | 22.850 | 0.9952 | 535.505 |
| | 333 | 1.643 | 3.593 | 0.8143 | 33.003 | 0.099 | 0.9245 | 7.065 | 1.192 | 0.939 | $1.35x10^{-6}$ | 23.282 | 0.9941 | 608.463 |
| MBC | 303 | 1.717 | 3.791 | 0.7287 | 32.362 | 0.098 | 0.8768 | 6.700 | 1.352 | 0.871 | $1.86x10^{-6}$ | 24.484 | 0.9446 | 519.115 |
| | 313 | 1.737 | 4.298 | 0.7252 | 34.483 | 0.107 | 0.8818 | 7.108 | 1.491 | 0.873 | $1.49x10^{-6}$ | 26.286 | 0.9304 | 578.343 |
| | 323 | 1.789 | 5.085 | 0.7217 | 35.971 | 0.128 | 0.9015 | 7.455 | 1.770 | 0.870 | $1.11x10^{-6}$ | 28.273 | 0.9216 | 669.962 |
| | 333 | 1.999 | 6.727 | 0.6668 | 37.736 | 0.161 | 0.9141 | 7.342 | 2.685 | 0.826 | $1.35x10^{-6}$ | 23.282 | 0.9941 | 608.463 |
| Ni-Al/MBC | 303 | 0.947 | 8.886 | 0.4347 | 45.455 | 0.174 | 0.7094 | 9.695 | 3.390 | 0.278 | $1.14x10^{-6}$ | 47.947 | 0.7273 | 661.480 |
| | 313 | 2.149 | 1.682 | 0.304 | 64.935 | 0.173 | 0.4297 | 10.917 | 6.133 | 0.373 | $2.61x10^{-7}$ | 36.728 | -0.0354 | 1384.348 |
| | 323 | 2.166 | 16.546 | 0.3213 | 66.225 | 0.223 | 0.5109 | 11.200 | 7.406 | 0.398 | $1.78x10^{-7}$ | 37.298 | -0.0376 | 1674.616 |
| | 333 | 2.267 | 19.404 | 0.2729 | 68.493 | 0.278 | 0.5014 | 11.275 | 10.357 | 0.298 | $1.89x10^{-7}$ | 50.729 | 0.0545 | 1628.016 |

magnetite biochar, the reactions become non-spontaneous. This may be explained by external influences on the system at both low and high temperatures. This phenomenon may be attributed to the solid temperature-dependent effect on the Gibbs free energy value, with the observed decrease possibly being caused by the system's work on the surroundings and the work of pressure forces.

### 3.6 BET Characterization Analysis

Relationships of BET with kinetics and isotherms include pore structure and pore diameter, affect the movement and diffusion of adsorbates in materials, determining the rate of velocity in determining the time to reach adsorption equilibrium, the surface area of which material is obtained can affect the maximum adsorption capacity, and the rate of adsorption, and provide information about surface sites available for adsorption. The results obtained for Ni-Al, magnetite biochar, and Ni-Al/magnetite biochar, as shown in Figure 8, follow the BET type IV isotherm model based on the IUPAC classification. Determination of the type IV isotherm is made by observing characteristics of type IV isotherm, which involves the formation of multilayer adsorption [61]. Data in Table 5 indicate that Ni-Al/magnetite biochar composite has the largest surface area and pore volume, which are 127.310 $m^2/g$ and 0.1950 $cm^3/g$, respectively, compared to precursor materials surface area, namely Ni-Al 5.845 $m^2/g$ and magnetite biochar 61.843 $m^2/g$. The smaller pore diameter of Ni-Al/magnetite biochar compared to Ni-Al and magnetite biochar is attributed to the presence of small-sized $Fe_3O_4$, which can increase the spacing between layers and block some micropores of LDH, resulting in the formation of larger mesopores. This is similar to previous research studies Ren *et al*. [62].

Table 4. Thermodynamic parameters for adsorption of methylene blue

| $C_o$ (mg/L) | T (K) | ΔH (kJ/mol) | | | ΔS (J/mol.K) | | | ΔG (kJ/mol) | | |
|---|---|---|---|---|---|---|---|---|---|---|
| | | Adsorbents | | | | | | | | |
| | | Ni-Al LDH | MBC | Ni-Al/MBC | Ni-Al LDH | MBC | Ni-Al/MBC | Ni-Al LDH | MBC | Ni-Al/MBC |
| 5 | 303 | 15.575 | 16.262 | 24.213 | 0.052 | 0.057 | 0.088 | 0.133 | -1.060 | -2.367 |
| | 313 | | | | | | | 0.651 | -1.631 | -3.244 |
| | 323 | | | | | | | -1.170 | -2.203 | -4.121 |
| | 333 | | | | | | | -1.688 | -2.775 | -4.998 |
| 15 | 303 | 5.749 | 22.952 | 24.757 | 0.027 | 0.087 | 0.101 | -2.516 | -3.415 | -5.896 |
| | 313 | | | | | | | -2.788 | -4.286 | -6.908 |
| | 323 | | | | | | | -3.061 | -5.156 | -7.920 |
| | 333 | | | | | | | -3.334 | -6.026 | -8.931 |
| 30 | 303 | 7.351 | 20.481 | 41.388 | 0.027 | 0.072 | 0.159 | -0.882 | -1.394 | -6.655 |
| | 313 | | | | | | | -1.154 | -2.116 | -8.240 |
| | 323 | | | | | | | -1.425 | -2.838 | -9.826 |
| | 333 | | | | | | | -1.697 | -3.560 | -11.411 |
| 45 | 303 | 7.878 | 11.405 | 41.531 | 0.024 | 0.038 | 0.155 | 0.607 | -0.098 | -5.438 |
| | 313 | | | | | | | 0.367 | -0.478 | -6.989 |
| | 323 | | | | | | | 0.127 | -0.857 | -8.539 |
| | 333 | | | | | | | -0.113 | -1.237 | -10.089 |
| 60 | 303 | 7.411 | 12.249 | 21.009 | 0.019 | 0.037 | 0.076 | 1.545 | 1.056 | -2.138 |
| | 313 | | | | | | | 1.362 | 0.687 | -2.902 |
| | 323 | | | | | | | 1.158 | 0.318 | -3.666 |
| | 333 | | | | | | | 0.964 | -0.052 | -4.430 |

Table 5. BET texture measurement results of materials

| Adsorbents | Surface Area ($m^2/g$) | Pore Volume ($cm^3/g$) | Pore Diameter (nm) |
|---|---|---|---|
| Ni/Al LDH | 5.845 | 0.004 | 4.546 |
| MBC | 61.843 | 0.1279 | 4.1368 |
| Ni-Al/MBC | 127.310 | 0.1950 | 3.0638 |

### 3.7 SEM-EDX Characterization Analysis

SEM analysis was used to determine the surface morphology, particle size and shape, purity, and homogeneity of the material to support adsorption ability in kinetic, isotherm, thermodynamic adsorption process, while EDX was used to determine the elemental content of the Ni-Al LDH adsorbent material, magnetite biochar, and Ni-Al/magnetite biochar LDH composite. The results of the SEM-EDX analysis are shown in Figure 9. Figure 9 (a) shows the morphological shape of Ni-Al as a large plate, has a rough surface, and has a typical structure of LDH, namely the presence of layered layers. The SEM results obtained are supported by the literature of Lesbani *et al*. [24]. Observation of the results of SEM magnetite biochar with a magnification of 500x in Figure 9 (b) shows that the material has a rough surface and an uneven, irregular shape that is in line with Fito *et al*. [63]. Ni-Al/magnetite biochar adsorbent contained in Figure 9 (c) displays the morphology of Ni-Al/magnetite biochar materials that stack on top of each other, thus forming large lumps. The stacking in the Ni-Al morphology indicates that there is space between layers that can exchange anions and is a typical structure of LDH. The large pores and non-uniform shape of the Ni-Al/magnetite biochar composite affect the adsorption capacity.

Table 6 shows the elements contained in the adsorbent material. Major compositions in LDH include carbon, oxygen, aluminum, silicon, and Ni. A high percentage of nickel ion weight is present on the surface interlayer of LDH. The magnetite biochar, there are elements of carbon and iron that have the highest percentage of weight, elements of Fe obtained from $Fe_3O_4$ materials. The composite material has all elements of the forming material, the presence of elements Cl and Na due to the addition of acids and bases in the coprecipitation process, and the percentage of oxygen weight is high due to agglomeration with carbon materials.

### 3.6 Adsorption Mechanism of Methylene Blue

Mechanisms for the interaction between methylene blue and composite in Figure 10 ac-

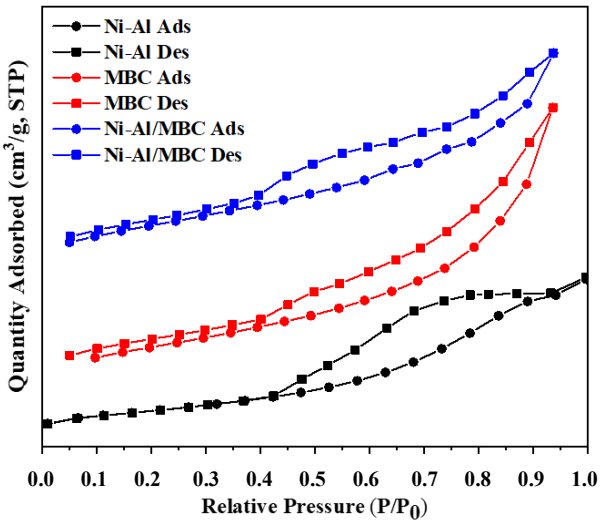


Figure 8. Nitrogen adsorption/desorption isotherm

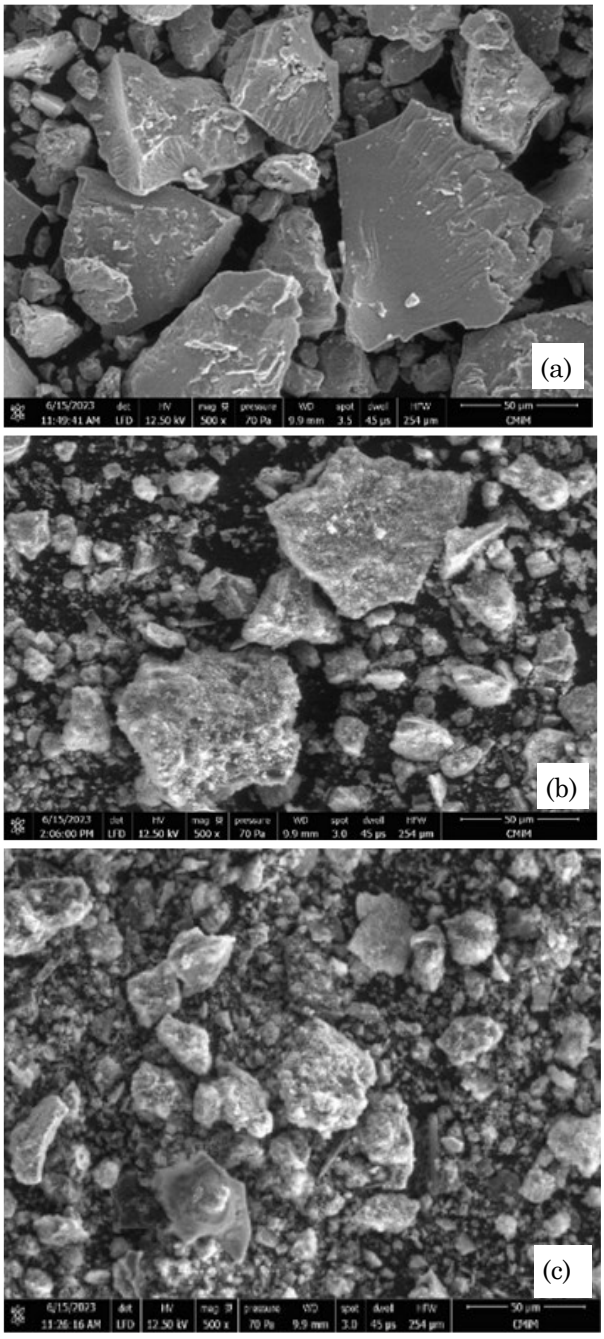


Figure 9. SEM images of (a) Ni-Al (b) Magnetite Biochar and (c) Ni-Al/magnetite biochar

cording to Kheradmand *et al.* [64]. Firstly, it involves hydrogen bonding interactions, i.e. interactions between hydrogen atoms and atoms with high electronegativity, such as oxygen, nitrogen, and fluorine. Secondly, there is an electrostatic interaction between the positively charged composite on Ni and Al metals and the chlorine groups on methylene blue, which are negatively charged, causing electrostatic attraction. In the $Fe_3O_4$ group, there is a hydroxyl group that allows protonated or deprotonation at specific pH pzc values, resulting in either a positive or negative charge. This phenomenon leads to the formation of electrostatic bonds with methylene blue, ultimately causing the removal of the dye. Third, phi-phi bonds exist, a bond between two carbon atoms in a triple bond in aromatic rings of biochar and methylene blue. Ni-Al/magnetite biochar has a porous structure, looking at the value found in SEM characterization for composite. It can result in methylene blue molecules entering, allowing the adsorption capacity to increase.

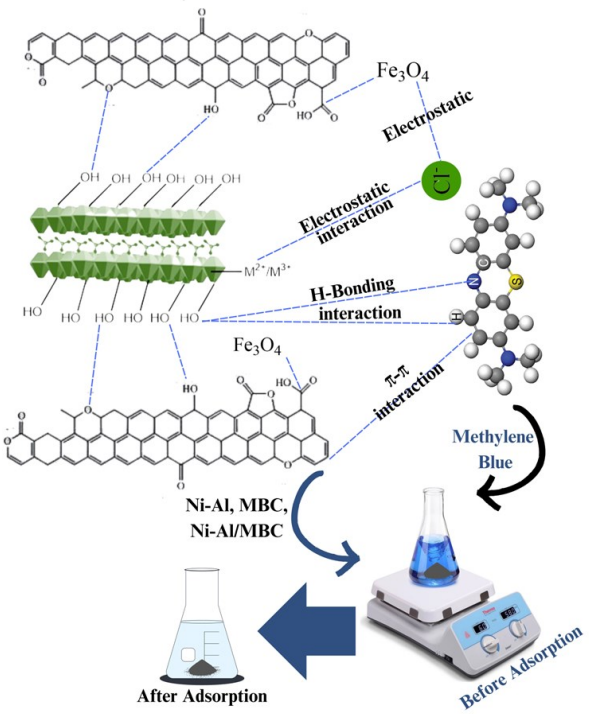


Figure 10. Adsorption mechanism of methylene blue

## 4. Conclusions

This study has conducted a successful synthesis of Ni-Al LDH and preparation of Ni-Al/magnetite biochar composite using the co-precipitation method in adsorbing methylene blue dye. Characterizations of XRD, FT-IR, BET, SEM-EDX, and VSM support the success of synthesis and preparation. Enhancement of adsorption capacity of adsorbents concerning physicochemical with the effectiveness of Ni-Al/magnetite biochar composite in repeated use for adsorption process has percent adsorption of 5 cycles, which are 96.587; 95.330; 93.293; 80.311; and 58.494 %. It proves that LDH adsorbent modified with magnetite biochar is potential and efficient in the treatment of methylene blue dye in solving aqueous environmental pollution. The enhancement of adsorption capacity and repeated use of adsorbents are related to physicochemical properties during the adsorption process at pH pzc 6 for composite. This was observed from the increase in composite surface area reaching 127.310 $m^2/g$ and magnetic saturation value of 8.35 emu/g. Due to the increase in surface area, the adsorption capacity of the composite was increased, with Qmax reaching 68.493 mg/g compared to $Q_{max}$ of LDH 33.003 mg/g and magnetite biochar 37.736 mg/g by following the Langmuir isotherm equation. The pseudo second order adsorption kinetics process took place with an $R^2$ value of 0.9993. Thermodynamics during the adsorption process is endothermic and spontaneous, which follows the physical adsorption process because of $\Delta H < 40$ kJ/mol.

## Acknowledgments

The authors would like to thank the Laboratory of Research Centre of Inorganic Materials and Complexes, Sriwijaya University, for the equipment and materials used during the research.

Table 6. EDX elemental composition analysis of materials

| Materials | Weight % | | | | | | | | Atomic % | | | | | | | |
|---|---|---|---|---|---|---|---|---|---|---|---|---|---|---|---|---|
| | C | O | Na | Al | Si | Cl | Fe | Ni | C | O | Na | Al | Si | Cl | Fe | Ni |
| Ni-Al LDH | 6.65 | 43.53 | - | 4.69 | 0.69 | - | - | 44.44 | 13.09 | 64.33 | - | 4.11 | 0.58 | - | - | 17.90 |
| MBC | 16.26 | 29.78 | - | 0.85 | 2.88 | - | 50.21 | - | 31.87 | 43.81 | - | 0.74 | 2.42 | - | 21.16 | - |
| Ni-Al/MBC | 23.20 | 34.93 | 1.97 | 1.82 | 7.04 | 0.71 | 10.88 | 19.44 | 38.14 | 43.11 | 1.69 | 1.33 | 4.95 | 0.39 | 3.85 | 6.54 |

## CRediT Author Statement

*Zaqiya Artha Zahara*: Investigation, Writing - Original Draft, Data Curation; *Idha Royani*: Writing - Review & Editing, Formal analysis; *Neza Rahayu Palapa*: Writing - Review & Editing, Visualization; *Risfidian Mohadi*: Validation, Writing - Review & Editing, Project administration; *Aldes Lesbani*: Conceptualization, Methodology, Supervision, Resources, Funding acquisition.

## References


[1] Adjid, G.A.F., Kurniawan, A., Nazriati (2022). Textile Industry Waste Pollution in The Konto River. *J .Exp. Life Sci.*, 12 (3), 2022. DOI: 10.21776/ub.jels.2022.012.03.05

[2] Lellis, B., Fávaro-Polonio, C.Z., Pamphile, J.A., Polonio, J.C. (2019). Effects of textile dyes on health and the environment and bioremediation potential of living organisms. *Biotechnology Research and Innovation*, 3(2), 275–290. DOI: 10.1016/j.biori.2019.09.001.

[3] Kuang, Y., Zhang, X., Zhou, S. (2020). Adsorption of methylene blue in water onto activated carbon by surfactant modification. *Water (Switzerland)*, 12(2), 1–19. DOI: 10.3390/w12020587.

[4] Yang, C., Dong, W., Cui, G., Zhao, Y., Shi, X., Xia, X., Tang, B., Wang, W. (2017). Highly efficient photocatalytic degradation of methylene blue by P2ABSA-modified $TiO_2$ nanocomposite due to the photosensitization synergetic effect of $TiO_2$ and P2ABSA. *RSC Advances*, 7 (38), 23699–23708. DOI: 10.1039/c7ra02423a.

[5] Khan, I., Saeed, K., Zekker, I., Zhang, B., Hendi, A.H., Ahmad, A., Ahmad, S., Zada, N., Ahmad, H., Shah, L.A., Shah, T., Khan, I. (2022). Review on Methylene Blue: Its Properties, Uses, Toxicity and Photodegradation. *Water (Switzerland)*, 14 (2) DOI: 10.3390/w14020242.

[6] Radoor, S., Karayil, J., Jayakumar, A., Parameswaranpillai, J., Siengchin, S. (2021). Release of toxic methylene blue from water by mesoporous silicalite-1: characterization, kinetics and isotherm studies. *Applied Water Science*, 11 (7), 1–12. DOI: 10.1007/s13201-021-01435-z.

[7] Oladoye, P.O., Ajiboye, T.O., Omotola, E.O., Oyewola, O.J. (2022). Methylene blue dye: Toxicity and potential elimination technology from wastewater. *Results in Engineering*, 16(September), 100678. DOI: 10.1016/j.rineng.2022.100678.

[8] Huang, R., Zhang, Q., Yao, H., Lu, X., Zhou, Q., Yan, D. (2021). Ion-exchange resins for efficient removal of colorants in bis(hydroxyethyl) terephthalate. *ACS Omega*, 6 (18), 12351–12360. DOI: 10.1021/acsomega.1c01477.

[9] Abid, M.F., Zablouk, M.A., Abid-Alameer, A.M. (2012). Experimental study of dye removal from industrial wastewater by membrane technologies of reverse osmosis and nanofiltration. *Journal of Environmental Health Science and Engineering*, 9(1), 1–9. DOI: 10.1186/1735-2746-9-17

[10] Visa, M. (2016). Synthesis and characterization of new zeolite materials obtained from fly ash for heavy metals removal in advanced wastewater treatment. *Powder Technology*, 294 (1), 338-347. DOI: 10.1016/j.powtec.2016.02.019

[11] Lou, T., Cui, G., Xun, J., Wang, X., Feng, N., Zhang, J. (2018). Synthesis of a terpolymer based on chitosan and lignin as an effective flocculant for dye removal. *Colloids and Surfaces A: Physicochemical and Engineering Aspects*, 537 (October 2017), 149–154. DOI: 10.1016/j.colsurfa.2017.10.012.

[12] Javeed Ganaie, R., Rafiq, S., Sharma, A. (2023). Recent Advances in Physico-chemical Methods for Removal of Dye from Wastewater. *IOP Conference Series: Earth and Environmental Science*, 1110 (1) DOI: 10.1088/1755-1315/1110/1/012040.

[13] C, L., G, A.G.R. (2019). A review on photodegradation of various dyes using photocatalysts. *International Journal of Advanced Scientific Research and Management*, 4 (7) DOI: 10.36282/ijasrm/4.7.2019.1584.

[14] Shabir, M., Yasin, M., Hussain, M., Shafiq, I., Akhter, P., Nizami, A.S., Jeon, B.H., Park, Y.K. (2022). A review on recent advances in the treatment of dye-polluted wastewater. *Journal of Industrial and Engineering Chemistry*, 112, 1–19. DOI: 10.1016/j.jiec.2022.05.013.

[15] Ullah, A., Zahoor, M., Din, W.U., Muhammad, M., Khan, F.A., Sohail, A., Ullah, R., Ali, E.A., Murthy, H.C.A. (2022). Removal of Methylene Blue from Aqueous Solution Using Black Tea Wastes: Used as Efficient Adsorbent. *Adsorption Science and Technology*, 2022. DOI: 10.1155/2022/5713077.

[16] Benjelloun, M., Miyah, Y., Akdemir Evrendilek, G., Zerrouq, F., Lairini, S. (2021). Recent Advances in Adsorption Kinetic Models: Their Application to Dye Types. *Arabian Journal of Chemistry*, 14 (4), 103031. DOI: 10.1016/j.arabjc.2021.103031.

[17] Jinisha, R., Gandhimathi, R., Ramesh, S.T., Nidheesh, P. V., Velmathi, S. (2018). Removal of rhodamine B dye from aqueous solution by electro-Fenton process using iron-doped mesoporous silica as a heterogeneous catalyst. *Chemosphere*, 200, 446–454. DOI: 10.1016/j.chemosphere.2018.02.117.

[18] Saigl, Z.M. (2021). Various adsorbents for removal of rhodamine b dye: A review. Indonesian Journal of Chemistry, 21(4), 1039–1056. DOI: 10.22146/ijc.62863.

[19] Boulahbal, M., Malouki, M.A., Canle, M., Redouane-Salah, Z., Devanesan, S., AlSalhi, M.S., Berkani, M. (2022). Removal of the industrial azo dye crystal violet using a natural clay: Characterization, kinetic modeling, and RSM optimization. *Chemosphere*, 306 (July), 135516. DOI: 10.1016/j.chemosphere.2022.135516.

[20] Bharath Balji, G., Surya, A., Govindaraj, P., Monisha Ponsakthi, G. (2022). Utilization of fly ash for the effective removal of hazardous dyes from textile effluent. *Inorganic Chemistry Communications*, 143 (June), 109708. DOI: 10.1016/j.inoche.2022.109708.

[21] Ngulube, T., Gumbo, J.R., Masindi, V., Maity, A. (2017). An update on synthetic dyes adsorption onto clay based minerals: A state-of-art review. *Journal of Environmental Management*, 191, 35–57. DOI: 10.1016/j.jenvman.2016.12.031.

[22] Tatarchuk, T., Soltys, L., Macyk, W. (2023). Magnetic adsorbents for removal of pharmaceuticals: A review of adsorption properties. *Journal of Molecular Liquids*, 384 (May), 122174. DOI: 10.1016/j.molliq.2023.122174.

[23] Palapa, N.R., Taher, T., Mohadi, R., Rachmat, A., Mardiyanto, M., Miksusanti, M., Lesbani, A. (2021). NiAl-layered double hydroxide intercalated with Keggin polyoxometalate as adsorbent of malachite green : kinetic and equilibrium studies. *Chemical Engineering Communications*, 0(0), 1–12. DOI: 10.1080/00986445.2021.1895773.

[24] Lesbani, A., Palapa, N.R., Sayeri, R.J., Taher, T., Hidayati, N. (2021). High reusability of NiAl LDH/biochar composite in the removal methylene blue from aqueous solution. *Indonesian Journal of Chemistry*, 21(2), 421–434. DOI: 10.22146/ijc.56955.

[25] Keyikoglu, R., Khataee, A., Yoon, Y. (2022). Layered double hydroxides for removing and recovering phosphate: Recent advances and future directions. Advances in Colloid and Interface Science, 300(December 2021), 102598. DOI: 10.1016/j.cis.2021.102598.

[26] Cao, Y., Wu, X., Li, B., Tang, X., Lin, X., Li, P., Chen, H., Huang, F., Wei, C., Wei, J., Qiu, G. (2023). Ca–La layered double hydroxide (LDH) for selective and efficient removal of phosphate from wastewater. *Chemosphere*, 325 (January), 138378. DOI: 10.1016/j.chemosphere.2023.138378.

[27] Jin, L., Zhou, X., Wen, J., Peng, L. (2022). A green route for the preparation of layered double hydroxides from basic magnesium carbonate. *Magnetic Resonance Letters*, 2(3), 177–185. DOI: 10.1016/j.mrl.2022.06.004.

[28] Normah, N., Juleanti, N., Siregar, P.M.S.B.N., Wijaya, A., Palapa, N.R., Taher, T., Lesbani, A. (2021). Size selectivity of anionic and cationic dyes using LDH modified adsorbent with low-cost rambutan peel to hydrochar. *Bulletin of Chemical Reaction Engineering & Catalysis*, 16 (4), 869–880. DOI: 10.9767/BCREC.16.4.12093.869-880.

[29] Tang, Y., Zhang, X., Li, X., Bai, J., Yang, C., Zhang, Y., Xu, Z., Jin, X., Jiang, Y. (2023). Facile synthesis of magnetic ZnAl layered double hydroxides and efficient adsorption of malachite green and Congo red. *Separation and Purification Technology*, 322 (May), 124305. DOI: 10.1016/j.seppur.2023.124305.

[30] Wijaya, A., Siregar, P.M.S.B.N., Priambodo, A., Palapa, N.R., Taher, T., Lesbani, A. (2021). Innovative Modified of Cu-Al/C (C = Biochar, Graphite) Composites for Removal of Procion Red from Aqueous Solution. *Science and Technology Indonesia*, 6 (4), 228–234. DOI: 10.26554/sti.2021.6.4.228-234.

[31] Pelalak, R., Hassani, A., Heidari, Z., Zhou, M. (2023). State-of-the-art recent applications of layered double hydroxides (LDHs) material in Fenton-based oxidation processes for water and wastewater treatment. *Chemical Engineering Journal*, 474 (August), 145511. DOI: 10.1016/j.cej.2023.145511.

[32] Karim, A. V., Hassani, A., Eghbali, P., Nidheesh, P. V. (2022). Nanostructured modified layered double hydroxides (LDHs)-based catalysts: A review on synthesis, characterization, and applications in water remediation by advanced oxidation processes. *Current Opinion in Solid State and Materials Science*, 26 (1), 100965. DOI: 10.1016/j.cossms.2021.100965.

[33] Shou, J., Jiang, C., Wang, F., Qiu, M., Xu, Q. (2015). Fabrication of $Fe_3O_4$/MgAl-layered double hydroxide magnetic composites for the effective decontamination of Co(II) from synthetic wastewater. *Journal of Molecular Liquids*, 207, 216–223. DOI: 10.1016/j.molliq.2015.03.047.

[34] Tamjidi, S., Esmaeili, H., Kamyab Moghadas, B. (2019). Application of magnetic adsorbents for removal of heavy metals from wastewater: A review study. *Materials Research Express*, 6(10), 102004. DOI: 10.1088/2053-1591/ab3ffb.

[35] Gholami, P., Dinpazhoh, L., Khataee, A., Hassani, A., Bhatnagar, A. (2020). Facile hydrothermal synthesis of novel Fe-Cu layered double hydroxide/biochar nanocomposite with enhanced sonocatalytic activity for degradation of cefazolin sodium. *Journal of Hazardous Materials*, 381 (April 2019), 120742. DOI: 10.1016/j.jhazmat.2019.120742.

[36] Hassan, M.R., Yakout, S.M., Abdeltawab, A.A., Aly, M.I. (2021). Ultrasound facilitates and improves removal of triphenylmethane (crystal violet) dye from aqueous solution by activated charcoal: A kinetic study. *Journal of Saudi Chemical Society*, 25 (6), 101231. DOI: 10.1016/j.jscs.2021.101231.

[37] Hu, X., Li, P., Zhang, X., Yu, B., Lv, C., Zeng, N., Luo, J., Zhang, Z., Song, J., Liu, Y. (2019). Ni-based catalyst derived from NiAl layered double hydroxide for vapor phase catalytic exchange between hydrogen and water. *Nanomaterials*, 9(12), 1688. DOI: 10.3390/nano9121688.

[38] Din, S.U., Khan, M.S., Hussain, S., Imran, M., Haq, S., Hafeez, M., Zain-ul-Abdin, Rehman, F.U., Chen, X. (2021). Adsorptive Mechanism of Chromium Adsorption on Siltstone–Nanomagnetite–Biochar Composite. *Journal of Inorganic and Organometallic Polymers and Materials*, 31(4), 1608–1620. DOI: 10.1007/s10904-020-01829-7.

[39] Siregar, P.M.S.B.N., Palapa, N.R., Wijaya, A., Fitri, E.S., Lesbani, A. (2021). Structural stability of ni/al layered double hydroxide supported on graphite and biochar toward adsorption of congo red. *Science and Technology Indonesia*, 6 (2), 85–95. DOI: 10.26554/STI.2021.6.2.85-95.

[40] Din, S.U., Azeez, A., Zain-ul-Abdin, Haq, S., Hafeez, M., Imran, M., Hussain, S., Alarfaji, S.S. (2021). Investigation on Cadmium Ions Removal from Water by a Nanomagnetite Based Biochar Derived from Eleocharis Dulcis. *Journal of Inorganic and Organometallic Polymers and Materials*, 31 (1), 415–425. DOI: 10.1007/s10904-020-01758-5.

[41] Manojkumar, M.S., Jeyajothi, K., Jagadeesan, A., Jeevanantham, V. (2022). Magnetic separation of green synthesized $Fe_3O_4$ nanoparticles on photocatalytic activity of methyl orange dye removal. *Journal of the Indian Chemical Society*, 99 (8), 100559. DOI: 10.1016/j.jics.2022.100559.

[42] Jun, B.M., Kim, Y., Han, J., Yoon, Y., Kim, J., Park, C.M. (2019). Preparation of activated biochar-supported magnetite composite for adsorption of polychlorinated phenols from aqueous solutions. *Water (Switzerland)*, 11 (9), 1–16. DOI: 10.3390/w11091899.

[43] Hairuddin, M.N., Mubarak, N.M., Khalid, M., Abdullah, E.C., Walvekar, R., Karri, R.R. (2019). Magnetic palm kernel biochar potential route for phenol removal from wastewater. *Environmental Science and Pollution Research*, 26 (34), 35183–35197. DOI: 10.1007/s11356-019-06524-w.

[44] Revellame, E.D., Fortela, D.L., Sharp, W., Hernandez, R., Zappi, M.E. (2020). Adsorption kinetic modeling using pseudo-first order and pseudo-second order rate laws: A review. *Cleaner Engineering and Technology*, 1 (October), 100032. DOI: 10.1016/j.clet.2020.100032.

[45] Kalam, S., Abu-Khamsin, S.A., Kamal, M.S., Patil, S. (2021). Surfactant Adsorption Isotherms: A Review. *ACS Omega*, 6(48), 32342–32348. DOI: 10.1021/acsomega.1c04661.

[46] Yadav, B.S., Dasgupta, S. (2022). Effect of time, pH, and temperature on kinetics for adsorption of methyl orange dye into the modified nitrate intercalated MgAl LDH adsorbent. *Inorganic Chemistry Communications*, 137 (January), 109203. DOI: 10.1016/j.inoche.2022.109203.

[47] Karaca, S., Gürses, A., Açişli, Ö., Hassani, A., Kiranşan, M., Yikilmaz, K. (2013). Modeling of adsorption isotherms and kinetics of Remazol Red RB adsorption from aqueous solution by modified clay. *Desalination and Water Treatment*, 51 (13–15), 2726–2739. DOI: 10.1080/19443994.2012.749368.

[48] Chen, X., Hossain, M.F., Duan, C., Lu, J., Tsang, Y.F., Islam, M.S., Zhou, Y. (2022). Isotherm models for adsorption of heavy metals from water - A review. *Chemosphere*, 307(P1), 135545. DOI: 10.1016/j.chemosphere.2022.135545.

[49] Sahmoune, M.N. (2019). Evaluation of thermodynamic parameters for adsorption of heavy metals by green adsorbents. *Environmental Chemistry Letters*, 17 (2), 697–704. DOI: 10.1007/s10311-018-00819-z.

[50] Al-Saeedi, S.I., Areej, A., Qamar, M.T., Alhujaily, A., Iqbal, S., Alotaibi, M.T., Aslam, M., Qayyum, M.A., Bahadur, A., Awwad, N.S., Jazaa, Y., Elkaeed, E.B. (2023). Isotherm and kinetic studies for the adsorption of methylene blue onto a novel $Mn_3O_4$-$Bi_2O_3$ composite and their antifungal performance. *Frontiers in Environmental Science*, 11 (May), 1–16. DOI: 10.3389/fenvs.2023.1156475.

[51] Gülen, J., Zorbay, F. (2017). Methylene Blue Adsorption on a Low Cost Adsorbent—Carbonized Peanut Shell. *Water Environment Research*, 89 (9), 805–816. DOI: 10.2175/106143017x14902968254836.

[52] Trifi, I.M., Trifi, B., Zendah, H., Hamrouni, B. (2021). Comparative removal of methylene blue from aqueous solution using different adsorbents. *Journal of the Chilean Chemical Society*, 66 (3), 5246–5250. DOI: 10.4067/S0717-97072021000305246.

[53] Ngapa, Y.D., Gago, J. (2021). Optimizing of Competitive Adsorption Methylene Blue and Methyl Orange using Natural Zeolite from Ende-Flores. *JKPK (Jurnal Kimia dan Pendidikan Kimia)*, 6(1), 39. DOI: 10.20961/jkpk.v6i1.46132.

[54] Cundari, L., Saputra, E., Suranto, A., Yandriani, Y., Rosalina, R. (2020). the Effect of Adsorbent Type and Ratio on Removal and Isotherm Adsorption of Methylene Blue. *Jurnal Sains Materi Indonesia*, 21 (3), 115. DOI: 10.17146/jsmi.2020.21.3.5900.

[55] Mohadi, R., Siregar, P.M.S.B.N., Palapa, N.R., Lesbani, A. (2022). Preparation of Zn/Al-chitosan Composite for the Selective Adsorption of Methylene Blue Dye in Water. *Makara Journal of Science*, 26(2), 128–136. DOI: 10.7454/mss.v26i2.1313.

[56] Vezentsev, A.I., Thuy, D.M., Goldovskaya-Peristaya, L.F., Glukhareva, N.A. (2018). Adsorption of methylene blue on the composite sorbent based on bentonite-like clay and hydroxyapatite. *Indonesian Journal of Chemistry*, 18 (4), 733–741. DOI: 10.22146/ijc.37050.

[57] Budnyak, T.M., Aminzadeh, S., Pylypchuk, I. V., Sternik, D., Tertykh, V.A., Lindström, M.E., Sevastyanova, O. (2018). Methylene Blue dye sorption by hybrid materials from technical lignins. *Journal of Environmental Chemical Engineering*, 6 (4), 4997–5007. DOI: 10.1016/j.jece.2018.07.041.

[58] Onigbinde, M.O., Fatoye, E.O., Isola, O.B. (2022). Methylene Blue Dye Adsorption in Aqueous System using Microcrystalline Cellulose obtained from Sugarcane Bagasse. *Journal of Applied Sciences and Environmental Management*, 26 (12), 1943–1950. DOI: 10.4314/jasem.v26i12.8.

[59] Ahmad, N., Suryani Arsyad, F., Royani, I., Lesbani, A. (2022). Adsorption of methylene blue on magnetite humic acid: Kinetic, isotherm, thermodynamic, and regeneration studies. *Results in Chemistry*, 4 (November), 100629. DOI: 10.1016/j.rechem.2022.100629.

[60] Arabkhani, P., Asfaram, A. (2020). Development of a novel three-dimensional magnetic polymer aerogel as an efficient adsorbent for malachite green removal. *Journal of Hazardous Materials,* 384 (September 2019), 121394. DOI: 10.1016/j.jhazmat.2019.121394.

[61] Abebe, B., Murthy, H.C.A., Amare, E. (2018). Summary on Adsorption and Photocatalysis for Pollutant Remediation: Mini Review. *Journal of Encapsulation and Adsorption Sciences*, 08 (04), 225–255. DOI: 10.4236/jeas.2018.84012.

[62] Ren, S., Wang, Y., Han, Z., Zhang, Q., Cui, C. (2022). Synthesis of polydopamine modified MgAl-LDH for high efficient Cr(VI) removal from wastewater. *Environmental Research*, 215 (P1), 114191. DOI: 10.1016/j.envres.2022.114191.

[63] Fito, J., Abewaa, M., Nkambule, T. (2023). Magnetite-impregnated biochar of parthenium hysterophorus for adsorption of Cr(VI) from tannery industrial wastewater. *Applied Water Science*, 13 (3), 1–23. DOI: 10.1007/s13201-023-01880-y.

[64] Kheradmand, A., Negarestani, M., Kazemi, S., Shayesteh, H., Javanshir, S., Ghiasinejad, H. (2022). Adsorption behavior of rhamnolipid modified magnetic Co/Al layered double hydroxide for the removal of cationic and anionic dyes. *Scientific Reports*, 12(1), 1–17. DOI: 10.1038/s41598-022-19056-0.